

# Scaled Spectroscopy of $^1S^e$ and $^1P^o$ Highly Excited States of Helium

B. Grémaud<sup>(a)</sup> and P. Gaspard

*Service de Chimie Physique and Center for Nonlinear Phenomena and Complex System,  
Université Libre de Bruxelles, Campus Plaine, Code Postal 231, Blvd du Triomphe, B-1050 Brussels, Belgium.*

(November 20, 2018)

In this paper, we examine the properties of the  $^1S^e$  and  $^1P^o$  states of helium, combining perimetric coordinates and complex rotation methods. We compute Fourier transforms of quantities of physical interest, among them the average of the operator  $\cos \theta_{12}$ , which measures the correlation between the two electrons. Graphs obtained for both  $^1S^e$  and  $^1P^o$  states show peaks at action of classical periodic orbits, either “frozen planet” orbit or asymmetric stretch orbits. This observation legitimates the semiclassical quantization of helium with those orbits only, not just for  $S$  states but also for  $P$  states, which is a new result. To emphasize the similarity between the  $S$  and  $P$  states we show wavefunctions of  $^1P^o$  states, presenting the same structure as  $^1S^e$  states, namely the “frozen planet” and asymmetric stretch configurations.

## I. INTRODUCTION

The helium atom is one of the prototypes of atomic systems showing chaotic behaviour at the classical level. Even if the non-integrability of the three-body problem has been known for a long time, major steps have been realized only during the last ten years, giving rise to a regain of activity in this field [1–9,9]. From a theoretical point of view, two reasons have contributed to recent advances. One of the reasons has been the development of powerful methods for the numerical resolution of the quantum problem along with the advent of modern computers. The other reason has been the emergence of an understanding of the quantum mechanics of classically chaotic systems, especially, by the developments of new semiclassical methods, which link the two different worlds [10]. In addition, from the experimental point of view, the most recent technologies have enabled very high resolution spectroscopy of the helium atom, reaching energy domains where different Rydberg series strongly overlap giving rise to chaotic behaviour [11–14]. As a consequence of all these studies, the helium atom is now quite well understood both from the quantum and the semiclassical point of view.

Still, the knowledge on this subject is poor compared to that of other atomic systems, like the hydrogen atom in a magnetic field or in a microwave field. For example, there are no systematic studies of the classical phase space, only a few types of periodic orbits are known. Surprisingly, these orbits suffice for the semiclassically quantization of the helium atom or of the negative hydrogen ion with quite a good agreement with *ab initio* quantum calculations [15,16,7,5]. One purpose of this paper is the validation of these results, by proceeding the other way round : extracting the classical information from the quantum properties. Although, this kind of study has already been conducted for a long time on many other chaotic systems, it does not exist for the helium atom. There are many reasons to explain this lack, among them the fundamental one is probably the high complexity of the numerical resolution of the full quantum problem ( all degrees of freedom and no approximations). The same is also true for the classical approach : a very large phase space (eight dimensional) and a dynamics which is never fully chaotic.

Through intensive numerics, we have been able to overcome these difficulties and to perform a semiclassical analysis of the helium spectrum, using the scaled Fourier transform method. Thus, we have been able to recover the actions of the collinear periodic orbits (both *eZe* and *Zee* configurations) from the  $L = 0$  states. As the experimentally accessible states are  $L = 1$  states, we applied the same method to them. Similar results have then been obtained, in agreement with the usual treatment of non-zero angular momentum states with  $L = 0$  periodic orbits. The similarity between the  $L = 0$  and  $L = 1$  states is emphasized by plotting wavefunctions of  $L = 1$  states, showing the same kind of structures, namely frozen-planet configuration or localization around the asymmetric stretch orbit.

The paper is organized as follows : In Sec. II we summarize the generalities about the quantum helium and its numerical resolution. In Sec. III, we describe the properties of the classical system. In Sec. IV we present the numerical scaled spectroscopy of  $^1S^e$  and  $^1P^o$  states, with wavefunctions of  $^1P^o$  states. These results and the conclusions are discussed in Sec. V.

## II. HELIUM: EXACT QUANTUM ANALYSIS

### A. Generalities

The schematic structure based on the independent electrons picture is rather simple : the first electron gives rise to a Rydberg series (the  $\text{He}^+$  levels) of simple ionization thresholds. The second electron creates further Rydberg series which converge to each of the simple ionization thresholds (see Fig. 1). The limit of the series of the simple ionization thresholds is the double ionization threshold. Above the first simple ionization threshold, all states are doubly excited states and because of the electron-electron interaction they become resonances : one electron can ionize as the other falls on a lower state. The first series remains discrete. The different series are labelled by the quantum number  $N$ , which is the principal quantum number of the  $\text{He}^+$  hydrogenic levels.

After the first experimental observations of the doubly excited states [17], it has become clear that this picture was unable to give any sensible quantum numbers. Many different systems have been proposed to label the states [18–27]. Here we only present the most frequently used, proposed by Herrick and Sinanoglu. Apart from the two obvious quantum number ( $L, M$ ) associated with the total angular momentum and its projection along an arbitrary fixed axis, they introduced three other quantum numbers ( $N, K, T$ ).  $N$  is the principal quantum number of the inner electron (the threshold label).  $T$  is the projection (actually, the absolute value) of the total angular momentum onto the inter-electronic axis.  $K$  is related to the projection of the difference of the two Runge-Lenz vectors on the inter-electronic axis. For very high excited states the quantum number  $K$  measures the angular correlation between the two electrons. Indeed, the expectation value of the operator  $\cos \theta_{12}$  in the  $|N, K, T\rangle$  states is  $-K/N$  for  $N$  large. Finally, an additional quantum number is added to label the behaviour of the states under the exchange of the two electrons.

### B. Perimetric coordinates

Different methods are used to solve numerically the non-relativistic three-body Coulomb problem [28–35]. Among these, the most efficient one is probably the combination of perimetric coordinates and complex rotation. This method is exact without any approximation and takes into account all the degrees of freedom. A complete review of it will be given in [36]. Not only does it provide the energies and the widths of the resonances, but it also allows us to compute any quantities of physical interest like oscillator strengths, wavefunctions... A short compilation is noted as follows :

The non-relativistic Hamiltonian, with infinite nucleus mass can be written in atomic units ( $\hbar = m_{e^-} = 4\pi\epsilon_0 = e^2 = 1$ ) as :

$$H = \frac{1}{2}(\mathbf{P}_1^2 + \mathbf{P}_2^2) - \frac{1}{r_1} - \frac{1}{r_2} + \frac{1}{Z} \frac{1}{r_{12}} \quad (1)$$

where the scaling  $\mathbf{r}_i \rightarrow Z\mathbf{r}_i$  has been carried out, so that for  $Z$  large, we are left with two independent hydrogen atoms perturbed by the term  $1/(r_{12}Z)$ . Because of this scaling, the eigenenergies of the Hamiltonian (1) must be multiplied by the factor  $Z^2$  to get the eigenenergies of the original system. For instance the ground state energy of helium ( $Z = 2$ ) is  $-0.725931094$  units in our energy scale (instead of  $-2.903724377$  a.u.).

The rotational invariance of  $H$  is used to separate the angular dependency of the wavefunction from the relevant dynamical variables, namely the three inter-particle distances. For a given pair of good quantum numbers ( $L, M$ ) (total angular momentum and its projection onto the  $z$ -axis of the fixed laboratory frame), the wavefunctions have the following expression :

$$\Psi_{LM} = \sum_{T=-L}^L \mathcal{D}_{MT}^{L*}(\psi, \theta, \phi) \Phi_T^{(LM)}(R, \rho, \zeta) \quad (2)$$

where  $(\psi, \theta, \phi)$  are Euler angles defined by the transformation of the original fixed frame to a molecular-like frame moving with the inter-electronic axis (see figure 2). The functions  $\mathcal{D}_{MT}^{L*}(\psi, \theta, \phi)$  are the matrix elements of the rotation operator in the  $L$  representation. They are eigenfunctions of the operators  $\{\mathbf{L}^2, L_z, L'_z\}$  for the eigenvalues  $\{L(L+1), M, T\}$ , where  $L'_z$  is the projection of the angular momentum along the inter-electronic axis. The three remaining variables  $(R, \rho, \zeta)$  are actually combinations of  $r_1$ ,  $r_2$  and  $r_{12}$ . All the information about the dynamics is thus contained in the various functions  $\Phi_T$ , which are coupled by Coriolis-like terms. The Hamiltonian  $H$  is then prediagonalized and we are left with effective Hamiltonians  $H_J$  in which all the angular variables are stripped

out. Eventually, these Hamiltonians become matrix Hamiltonians. Finally, the two discrete symmetries (parity and exchange of the two electrons) add relations between the functions  $\Phi_T$ . For example, the  $\mathbf{S}$  states have only one component  $\Phi(= \Phi_0)$ , which can be chosen symmetric ( $^1\mathbf{S}^e$  states) or antisymmetric ( $^3\mathbf{S}^e$  states). On the other hand, the  $\mathbf{P}$  states are described by three components  $\{\Phi_T\}_{T=0,\pm 1}$ . The  $\mathbf{P}$  states separate between odd and even states and finally, for odd states, the *a priori* three independent  $\Phi_T$ 's reduce to only one component, but with no more symmetry with respect to the exchange of the two electrons.

Although the molecular-like coordinates  $(R, \rho, \zeta)$  are useful to exploit the rotational invariance, they are not suitable for the numerical implementation. To overcome this difficulty, the well-known perimetric coordinates are introduced :

$$\begin{cases} x = & r_1 + r_2 - r_{12} \\ y = & r_1 - r_2 + r_{12} \\ z = & -r_1 + r_2 + r_{12} \end{cases} \quad (3)$$

Their domains of variation range from 0 to  $+\infty$  and are independent. (In contrast, we would have the condition  $|r_1 - r_2| \leq r_{12} \leq r_1 + r_2$  between  $r_1, r_2$  and  $r_{12}$ ).

The effective Hamiltonians are then expanded in the product of three ‘‘Sturmian’’ basis, one for each perimetric coordinates. The basis functions have the following expression :

$$\phi_n^{\alpha_u}(u) = \sqrt{\alpha_u} L_n(\alpha_u u) e^{-\frac{\alpha_u}{2} u} \quad (4)$$

where  $u$  is one of the perimetric coordinates  $(x, y, z)$ ,  $n$  a positive integer,  $\alpha_u$  a real parameter (the scaling or dilatation parameter) and  $L_n$  the  $n^{\text{th}}$  Laguerre polynomial. These functions are associated with the representation of the group  $SO(2, 1)$  formed by the following operators :

$$\begin{cases} S_3^{\alpha_u} = -\frac{1}{\alpha_u} \left[ u \frac{\partial^2}{\partial u^2} + \frac{\partial}{\partial u} \right] + \alpha_u \frac{u}{4} \\ S_1^{\alpha_u} = \frac{1}{\alpha_u} \left[ u \frac{\partial^2}{\partial u^2} + \frac{\partial}{\partial u} \right] + \alpha_u \frac{u}{4} \\ S_2^{\alpha_u} = i \left[ u \frac{\partial}{\partial u} + \frac{1}{2} \right] \end{cases} \quad (5)$$

Thanks to their group properties, these operators have selection rules in the Sturmian basis and the few non-zero matrix elements are analytically known. As the effective Hamiltonians are polynomial functions of the nine operators  $S_i^u$  ( $i = 1, 2, 3$  and  $u = x, y, z$ ), they also have selection rules. For  $\mathbf{S}$  (resp.  $\mathbf{P}^o$ ) states there are only 57 (resp. 215) non-zero matrix elements whose expressions are also given by polynomials. The representations of the  $H_J$  in the Sturmian basis are then infinite sparse banded matrices, which can be efficiently diagonalized (after truncation) using the Lanczos algorithm. This iterative method is extremely efficient for computing few eigenvalues of a very large banded matrix (typically 100 for a  $10000 \times 10000$  matrix with bandsize equal to 1000) in a very short time ( $\simeq 10$  minutes CPU on a usual workstation).

### C. Complex rotation

As stated in Section II A, above the first threshold of simple ionization, all the states are resonances. The complex rotation method is appropriate to compute directly the properties of these resonances (energy, width). Its properties rely on deep mathematical properties of the analytic continuation of the Green function in the complex plane [37,38]. A recent review of its application to atomic physics can be found in Ref. [39].

The method is included in our case by making the scaling parameters  $\alpha_u$  complex, more precisely  $\alpha_u \rightarrow \alpha_u e^{-i\theta}$ , where  $\theta$  is a real parameter (the rotation angle). The matrix representations of the Hamiltonians then become complex symmetric, but are no more Hermitian. The fundamental properties of the complex spectra are (see Fig. 3) :

- The bound states are still on the real axis.
- The continua are rotated by an angle  $2\theta$  on the lower-half complex plane, around their branching point.

- Each complex eigenvalue  $E_i$  gives the properties of one resonance, i.e. the energy is the real part of  $E_i$ , and the width is two times the negative of the imaginary part. The complex eigenvalues are independent of  $\theta$ , provided that they are not covered by the continua.

Therefore, the rotated Green function  $G(\theta)$  associated with  $H(\theta)$  has no longer a branch cut along the real axis and thus directly gives the analytic continuation of the original Green function in the complex lower half-plane. For a negative value of  $\theta$ , one obtains the analytic continuation in the upper half-plane. Furthermore, the eigenbasis of  $H(\theta)$  satisfies the two properties of closeness and orthogonality (for a non-Hermitian scalar product), and is thus used to express all the physical quantities originally written in the eigenbasis of  $H$ . For example, the one-photon photoionization cross-section from the ground state is given by :

$$\sigma(\omega) = \frac{4\pi\omega}{c} \text{Im} \sum_i \frac{\langle \overline{E_{i\theta}} | R(\theta) T | g \rangle^2}{E_{i\theta} - E_g - \hbar\omega} \quad (6)$$

where  $\hbar\omega$  is the photon energy,  $E_g$  is the ground state energy and  $T$  is the dipole operator. The main difference between the usual expression ( $\frac{4\pi\omega}{c} |\langle E | T | g \rangle|^2$ ) and formula (6) is the contribution of all eigenstates  $|E_{i\theta}\rangle$  of  $H(\theta)$  rather than only the continuum state  $|E\rangle$  of  $H$ . There are other little differences due to the non-Hermiticity of  $H(\theta)$  : for instance the complex conjugate of  $\langle E_{i\theta} |$ ,  $\langle \overline{E_{i\theta}} |$  and the square of the matrix element (not the modulus square) enter the formula (6). Also, the presence of the operator  $R(\theta)$  is necessary to backward-rotate  $\langle \overline{E_{i\theta}} |$  onto the real axis. A consequence is that for an uncovered resonance, the matrix element  $\langle \overline{E_{i\theta}} | R(\theta) T | g \rangle$  is independent of  $\theta$ , enlightening the underlying analytic properties of the Green function. On the contrary, the matrix element  $\langle \overline{E_{i\theta}} | T | g \rangle$  is  $\theta$ -dependent and has thus no clear physical meaning, although some interpretations have recently been extracted [40]. In principle, for a given energy  $E$ , only the total sum has a physical meaning, but for a well-isolated resonance  $E_{i\theta}$  (whose width is much smaller than the distance in energy to the other ones) and for  $E \simeq \text{Re}(E_{i\theta})$ , the main contribution comes from this resonance only with a Fano profile shape, whose  $q$ -parameter is given by :

$$q = - \frac{\text{Re} \langle \overline{E_{i\theta}} | R(\theta) T | g \rangle}{\text{Im} \langle \overline{E_{i\theta}} | R(\theta) T | g \rangle} \quad (7)$$

Finally, in the general case, thanks to the energy denominators, only the resonances with energies close to the energy  $E = E_g + \hbar\omega$  will contribute to the sum, which allows a numerical efficiency.

The complex rotation method can also be used to compute the probability density of a continuum state of energy  $E$ , through the following formula :

$$|\Psi_E(\mathbf{r})|^2 = \langle \mathbf{r} | E \rangle^2 = \frac{1}{\pi} \sum_i \frac{\langle \mathbf{r} | R(-\theta) | E_{i\theta} \rangle^2}{E_{i\theta} - E} \quad (8)$$

Again, for a well-isolated resonance, the main contribution of the preceding sum [at the energy  $E = \text{Re}(E_{i\theta})$ ] comes from this resonance, more precisely :

$$|\Psi_{E \sim E_{i\theta}}(\mathbf{r})|^2 \sim \frac{1}{\pi |\text{Im}(E_{i\theta})|} \text{Re}[\langle \mathbf{r} | R(-\theta) | E_{i\theta} \rangle^2] \quad (9)$$

which may thus be interpreted as the probability density of one resonance. Again, the backward rotation is essential to obtain sensible results and to provide physical interpretation.

### III. HELIUM: SEMI-CLASSICAL ANALYSIS

#### A. Periodic orbits

The main difficulty of the classical dynamics of the helium atom is the dimension of the phase space. Even for  $L = 0$  trajectories, the number of degrees of freedom is three, so that usual techniques like Poincaré surfaces of section are of no help. For non-zero angular momentum, there is another degree of freedom, which further increases the complexity. A systematic study of the classical dynamics is still needed. Another singularity is that the motion is never bounded,

even for negative energies. Thus classically, one electron can ionize at any energy, in contrast to the quantum problem for which exact bound states do exist. All this explains why so few periodic orbits are known.

Two classes of periodic orbits have already been widely explored : the collinear orbits and orbits on the Wannier ridge [2,41,16]. The latter is of relatively little interest with respect to the quantum problem (at least for  $N \leq 10$ , see Ref. [16]). On the contrary, the first class has been extensively used for the semiclassical quantization. For these orbits, the two electrons and the nucleus stay on the same axis at all times. They are of two types according to whether the electrons are on the same side of the nucleus or on opposite sides.

When the electrons are on opposite sides, the classical orbits are asymmetric stretches made of successive rebounds of one or the other electron on the nucleus. This simple scheme is used to encode the periodic orbits and, thus, to semiclassically quantize the helium atom through cycle-expansion techniques [15,8]. These orbits are unstable with respect to collinear perturbation and stable for perturbation in the other directions.

When the electrons are on the same side of the nucleus, there exists one periodic orbit, the now well-known frozen-planet configuration, which is surprisingly stable with respect to perturbations in any directions. The motion of the two electrons is extremely different from the asymmetric stretches : the outer electron is dynamically frozen at a large distance from the nucleus, while the inner electron oscillates in the electric field produced by the outer one. The torus quantization of this orbit has been fruitful to explain the long-lived resonances of the helium atom [15].

In Table I, we give the reduced actions ( $S_p/2\pi$ ) and others properties of the various periodic orbits.

## B. Scaling law and Fourier transform

The connection between the quantum and the classical worlds is made, in the case of a classically chaotic systems, by the Gutzwiller trace formula, which expresses the oscillating part of the density of states as an (infinite) sum over all unstable periodic orbits and their repetitions involving classical quantities only [10,42]. This formula is a particular case of the following more general expression :

$$\text{tr} \frac{\hat{A}}{E - \hat{H}} \Big|_{\text{osc}} = \frac{1}{i\hbar} \sum_{p,r} \left( \oint_p A_W dt \right) \frac{\exp \left[ \frac{i}{\hbar} r S_p(E) - i \frac{\pi}{2} r \mu_p \right]}{|\det(\mathbf{m}_p^r - \mathbb{1})|^{1/2}} \quad (10)$$

where  $\hat{A}$  is an arbitrary operator ( $\cos \theta_{12}$  in our case) and  $A_W$  is its Weyl-Wigner representation.  $S_p(E)$  is the reduced action of the periodic orbit  $p$  at the energy  $E$ ,  $\mu_p$  is its Maslov index, and  $\mathbf{m}_p$  is the monodromy matrix associated with this orbit. For  $\hat{A} = \mathbb{1}$ , we recover the usual oscillatory part of the density of states.

The scaling law of the Coulombian dynamics gives directly the dependence of the reduced action with respect to the energy. For  $E < 0$  we have :

$$S_p(E) = \frac{1}{\sqrt{-E}} S_p(-1) = \frac{1}{\sqrt{-E}} S_p \quad (11)$$

Thus, any periodic orbit at a negative energy  $E$  is mapped onto the same orbit at energy equal to  $-1$ . The right-hand member of equation (10) becomes :

$$\frac{1}{(-E)^{3/2}} \sum_{r,p} \mathcal{A}(r,p) \exp \left[ \frac{i}{\hbar} \frac{1}{\sqrt{-E}} r S_p(-1) \right] \quad (12)$$

In the preceding expression,  $\mathcal{A}$  denotes an amplitude factor independent of the energy. We also recover the result that the semiclassical limit is reached when  $E$  goes to zero, i.e., for very highly excited states.

Furthermore, by taking the Fourier transform of  $\text{tr} \frac{\hat{A}}{E - \hat{H}}$ , with respect to the variable  $1/\sqrt{-E}$ , we should obtain peaks at the scaled reduced actions  $S_p$  of the periodic orbits and their repetitions : This method is called the scaled spectroscopy and has already shown its power in many other chaotic systems.

## IV. NUMERICAL RESULTS

## A. Numerical implementation

For numerical purpose, we have to truncate the Sturmian basis. Since a basis vector is labelled with the three quantum number  $(n_x, n_y, n_z)$ , we truncate the basis with  $n_x + n_y + n_z \leq N_{\max}$ . We also work with  $\alpha = 2\beta = 2\gamma$  where  $\alpha = \alpha_x$ ,  $\beta = \alpha_y$ , and  $\gamma = \alpha_z$  are the three dilatation parameters of the basis functions (4). This choice gives a good asymptotic behaviour of the wavefunction for large values of both  $r_1$  and  $r_2$ . This choice also introduces additional selection rules, which therefore increase the sparseness of the matrices. For the  $^1\mathbf{S}^e$  states, we can also symmetrize the basis and consider  $|n_x, n_y, n_z\rangle + |n_x, n_z, n_y\rangle$ . We have considered truncations up to  $N_{\max} = 58$ , which gives a basis size equal to 18445 and a bandsize equal to 932. On a CRAY J90, the codes typically take 1000 seconds to run. For the  $^1\mathbf{P}^o$  states, we have also carried out the numerical calculation up to  $N_{\max} = 58$  where the basis size is equal to 35990 and the bandsize is equal to 3056. Here, the codes take 2000 seconds of CPU time to run on a CRAY C98. The convergence of the results have been checked with systematic variation of the basis size, of the complex-rotation angle  $\theta$ , and of the dilatation parameter  $|\alpha_u|$ .

## B. Photoionization cross-section

For the comparison with the experiments, the photoionization cross-section from the ground state is a suitable quantity for many different reasons. The first one is the existence of high quality experimental results [13,14], especially in the region where series strongly overlap. Furthermore, at the experimental resolution, neither the QED nor relativistic effects are resolved, so that no correction needs to be added to our results, in the present stage of experimental accuracy. Finally, because the cross-section involves the computation of the (complex) oscillator strengths, it will test not only the good convergence of the complex eigenenergies, but also of the good implementation of the backward rotation and the overlaps between eigenvectors computed at different scaling parameters, which is far from obvious [36]. Especially, the Fano  $q$ -parameter values are strongly dependent on the backward rotation.

Our results are based on the infinite nucleus-mass Hamiltonian. The corrections are taken into account by using the effective double ionization threshold value and the Rydberg constant value given in Ref. [14]. Furthermore, we have convoluted our “infinite precision” cross-section with a Lorentzian of width equal to the experimental resolution. Fig. 4 gives our numerical cross-section below the  $N = 5$  threshold where oscillations due to the interference with the lowest members of the  $N = 6$  series appears. The agreement with the figure of Ref. [13] is very good. We emphasize that there are no adjustable parameters. To make a better comparison, we give in Table II all the characteristic quantities (energy, reduced linewidth, reduced probability transition, Fano  $q$ -parameter, value of the inter-electronic angle) we have calculated in this energy range for the two principal series  $5, 3_n$  and  $5, 1_n$ . Even if still valid, Herrick’s classification starts to partially break up, as one can see in Fig. 5, where  $-\langle \cos \theta_{12} \rangle N$  is plotted versus the effective quantum number  $n_{\text{eff}}$ . This kind of plot has already been observed and analysed in Ref. [9]. Thus, the conclusion of Ref. [9] extends to the  $^1\mathbf{P}^o$  states, which is of great interest since the  $^1\mathbf{P}^o$  states are accessible in the current experiments. A more complete description of the photoionization cross-section will be given in Ref. [43].

## C. Scaled spectroscopy

As explained in the Introduction, one of our goals is to retrieve the classical quantities from the quantum ones. Thus, we have applied the scaled Fourier transform (SFT) techniques to the trace of the Green function (i.e. the density of states) and also to the trace of the operator  $G(E) \times \cos \theta_{12}$ , which characterizes the electron-electron correlations. Furthermore, since the function  $\theta \rightarrow \cos \theta$  has zero derivative for  $\theta = 0$  or  $\theta = \pi$ , it enhances the weight of the collinear orbits. The SFT is convoluted with a Welch window in order to lower the effects of the finite size of our spectrum.

Fig. 6 depicts the different results obtained for the  $^1\mathbf{S}^e$  and  $^1\mathbf{P}^o$  states. At the top, the SFT of the density only is shown, the  $^1\mathbf{S}^e$  case being on the right-hand side. The vertical lines indicate the scaled classical action of the frozen-planet periodic orbit ( $Zee$  configuration) and their repetitions. For both the  $^1\mathbf{S}^e$  states and the  $^1\mathbf{P}^o$  states, the SFT clearly has peaks at those classical actions. The fact that the  $Zee$  orbit is the only one visible is probably related to its stability in all directions. At the bottom of Fig. 6, we plotted the SFT of  $G(E) \times \cos \theta_{12}$ . The peaks at the  $Zee$  orbit have been lowered and some have disappeared. For the  $^1\mathbf{S}^e$  states, we see new dominant peaks at the classical actions of the three first asymmetric stretch orbits ( $eZe$  configuration). For the  $^1\mathbf{P}^o$  states, we also see new dominant peaks we can associate with the  $eZe$  asymmetric stretch orbits. However, the agreement is not so good because the peaks are slightly shifted although the  $eZe$  orbits are still emerging from the quantum data. In all these plots, the shifts tends to decrease, when increasing the number of eigenvalues used to compute the traces.

The fact that peaks at  $L = 0$  orbits are obtained for  $L \neq 0$  might be surprising, but this can be explained from a semi-classical point of view. For a given value of the quantum total angular momentum, we obtain an effective Hamiltonian acting only on the radial coordinates, in which centrifugal potentials (inverse square) appear. Taking the classical equivalent of this Hamiltonian and using the Coulomb scaling law, we directly obtain that these potentials vanish as  $|E| \rightarrow 0$ . This means that their contributions to the classical dynamics become negligible for energies close to the double ionisation threshold and we are left with the  $L = 0$  classical Hamiltonian.

Finally, we point out that neither the Wannier orbit nor the Langmuir orbit have appeared in our scaled spectroscopy. According to reference [16], the later orbit should contribute only for states above the  $N = 10$  threshold, which would explain that it is not observed in our study. The fact that we find peaks only at the collinear orbits can provide an explanation for the efficiency of the previous semiclassical quantizations [1,3,15], which are thus legitimized by our scaled spectroscopy analysis. Furthermore, our results support the hypothesis that the semiclassical quantization of the  $^1\mathbf{P}^o$  states can in principle be achieved with these collinear orbits only. Accordingly, the non-zero angular momentum states could be semiclassically quantized starting from these  $L = 0$  orbits.

#### D. Wavefunctions

The similarity between the  $^1\mathbf{P}^o$  and the  $^1\mathbf{S}^e$  states can be displayed by looking at the wavefunctions. For the  $^1\mathbf{S}^e$  states, there are only three internal degrees of freedom, namely the three interparticle distances and there is no angular dependency. This is no longer the case for the  $^1\mathbf{P}^o$  states, in which the angular part is not constant (but given by the three rotation matrix elements  $\mathcal{D}_{0T}^{1*}$ ). To allow pertinent comparison, we then trace the wavefunctions over the angular variables and study the dependencies with respect to the three remaining degrees of freedom.

Since our scaled spectroscopy has shown the important role of collinear configurations, we consider for our comparison the resonances satisfying the two criterions : (1) the value of  $\cos\theta_{12}$  has to be close to 1 or  $-1$ ; (2) the width is small compared to the distances to the neighbouring states. This last condition allows us to give a sense to the corresponding wavefunction because the resonance is long-lived and isolated. Selecting wavefunctions according to the two above criteria, we find that the resonances separate rather clearly into the two classes already observed for the  $^1\mathbf{S}^e$  states, namely the frozen-planet configuration for which the two electrons are on the same side of the nucleus and the asymmetric stretch configuration for which the two electrons are localized on the opposite sides.

Fig. 7 depicts the lowest frozen-planet state in the series  $N = 7$ . Its energy is  $-0.0113416$  atomic units (77.77 eV above the helium ground state), its width is  $1.38 \times 10^{-6}$  (0.15 meV). The real part of the value of  $\cos\theta_{12}$  is 0.73, the imaginary part being hundred times smaller. The figure shows the conditional density probability of the inner electron with respect to the fixed axis  $\mathbf{R}$  between the nucleus and the outer electron. The distance  $\mathbf{R}$  is given by the classical expectation value of the outer electron along the classical periodic orbit. Following the notation of Ref. [6], this state is  $(n, k, l) = (6, 0, 0)$ . These integers are the semiclassical quantum numbers in the EBK quantization of the tori surrounding the periodic orbit.  $n$  gives the number of nodes along the orbit, while  $k$  and  $l$  are related the stable motion perpendicular to the orbit. More precisely,  $k$  is the quantum number associated with the bending degree of freedom and  $l$  is associated with the stability of the orbit with respect to perturbation preserving the collinearity. In this figure, we see clearly the localization of the inner electron on the same side of the nucleus. This figure compares very well with the corresponding figures of Ref. [6].

Furthermore, Fig. 8 depicts a state in the  $N = 7$  series ( $E = -0.011564$  in atomic units or 77.75 eV above the helium ground state) with a very small width ( $\Gamma = 8.60 \times 10^{-9}$  a.u. or 0.936  $\mu\text{eV}$ ). But, the value of  $\cos\theta_{12}$  is in this case equal to  $-0.842$ . The electrons are essentially on the opposite side of the nucleus. Thus, we have plotted the wavefunction in the  $(r_1, r_2)$  plane for fixed inter-electronic angle  $\theta_{12} = \pi$ . The maximum of probability is clearly localized around the  $-$  asymmetric stretch orbit, shown on the top of the figure. Again this figure is comparable to those obtained for  $\mathbf{S}$  states, for example in Ref. [3].

#### V. CONCLUSIONS

In this paper, we carried out an *ab initio* study of the  $^1\mathbf{S}^e$  and  $^1\mathbf{P}^o$  states of helium, for which we have systematically calculated and characterized the main resonances and associated wavefunctions. Moreover, we have performed a semiclassical analysis by a numerical scaled spectroscopy, which reveals the main periodic orbits emerging out of the wave dynamics. In order to probe the correlation between the two electrons, we have studied, not only the mean level density and the photoionization cross-section, but also the mean values of  $\cos\theta_{12}$  where  $\theta_{12}$  is the angle between the positions of both electrons with respect to the nucleus. The scaled spectroscopy based on this quantity provides evidence for the collinear periodic orbis of both the  $eZe$  and the  $Zee$  configurations.

Although the families of the  $^1S^e$  and  $^1P^o$  states are ruled by different sets of partial differential equations derived from the Schrödinger equation, the present study reveals a strong similarity between these families, which can be explained by the difference of only one quantum of angular momentum between them whereas they are highly excited in energy. In particular, periodic orbits emerge at comparable values of the scaled reduced actions  $S_p$  for both families. This result is of great importance because it shows that both families have similar semiclassical properties and that their semiclassical quantization can in principle be carried out with collinear orbits of the same kind. This conclusion is further supported by the comparison between the resonant wavefunctions of the both families of states.

Moreover the calculated photoionization cross-section for the  $^1P^o$  states is in very good agreement with the recent experimental observations of Refs. [14]. The observed overlap of the  $N = 5$  series with states of the  $N = 6$  series is a quantum signature of the transition to a classically chaotic regime, which is at the origin of a partial breakdown of Herrick's classification scheme based on an integrable model. When the overlapping of the Rydberg series becomes important, Wigner repulsions between the states are known to induce irregularities in the resonance spectrum. In this regard, the emerging periodic orbits revealed by the scaled spectroscopy provide a complementary method to disclose ordered structures in highly congested spectra like those of doubly-excited helium.

### Acknowledgements

It is our pleasure to thank Prof. G. Nicolis for support of this research. P. G. is financially supported by the National Fund for Scientific Research (F.N.R.S. Belgium). During this research, B. G. has been financially supported by a fellowship of the European Commission under contract No. ERBCHBICT941418. Part of this research has also been supported by the ARC project "Quantum Keys for Reactivity" of the "Communauté française de Belgique" and by the project "Chaos and quantum mechanics in mesoscopic systems" of the "Banque Nationale de Belgique".

<sup>(a)</sup> Present Address : Laboratoire Kastler Brossel  
 Université Pierre et Marie Curie Tour 12 Etage 1  
 4, place Jussieu  
 F-75252 Paris cedex 05

- [1] Richter K. and Wintgen D., J. Phys. B **23**, L197 (1990)
- [2] Richter K. and Wintgen D. J. Phys. B: At. Mol. Opt. Phys. **23** L197 (1990)
- [3] Ezra G.S., Richter K., Tanner G. and Wintgen D., J. Phys. B **24**, L413 (1991)
- [4] Blümel R. and Reinhard W.P. Direction in Chaos **4** (1991)
- [5] Richter K. and Wintgen D., J. Phys. B: At. Mol. Opt. Phys. **24** L565 (1991)
- [6] Richter K., Briggs J.S., Wintgen D. and Solov'ev E.A., J. Phys. B: At. Mol. Opt. Phys. **25** 3929 (1992)
- [7] Gaspard P. and Rice S.A. Phys. Rev. A **93** 54 (1993)
- [8] Tanner G. and Wintgen D. Phys. Rev. Lett. **75** 2928 (1995)
- [9] Bürgers A., Wintgen D., and Rost J.M. J. Phys. B: At. Mol. Opt. Phys. **28** 3163 (1995)
- [10] *Chaos in Classical and Quantum Mechanics* Gutzwiller M.C. Springer-Verlag (1990)
- [11] Domke M., Xue C., Puschmann A., Mandel T., Hudson E. Shirley D.A., Kaindl G., Greene C.H., Sadeghpour H.R. and Petersen H. Phys. Rev. Lett. **66** 1306 (1991)
- [12] Domke M., Remmers G., and Kaindl G. Phys. Rev. Lett. **69** 1171 (1992)
- [13] Domke M., Schulz K., Remmers G., Kaindl G., and Wintgen D., Phys. Rev. A, **53**, 1424 (1996)
- [14] Schultz K., Kaindl G. Domke M. Bozek J.D. Heimann P.A. Schlachter A.S. and Rost J.M. Phys. Rev. Lett. **77** 3086 (1996)
- [15] Wintgen D., Richter K., and Tanner G., Chaos **2**, 19 (1992)
- [16] Müller J., Burgdörfer J., and Noid D., Phys. Rev. A **45**, 1471 (1992)
- [17] Madden R.P. and Codling K. Phys. Rev. Lett. **10** 516 (1963)
- [18] Sinanoglu O. Herrick D. R. J. Chem. Phys. **62** 886 (1973)
- [19] Herrick D.R. Phys. Rev. A **12** 413 (1975)
- [20] Herrick D.R. and Sinanoglu O. Phys. Rev. A **11** 97 (1975)
- [21] Herrick D.R. Phys. Rev. A **17** 1 (1978)
- [22] Herrick D.R. and Poliak R.D. J. Phys. B: At. Mol. Opt. Phys. **13** 4533 (1980)
- [23] Herrick D.R. Adv. Chem. Phys. **52** 1 (1983)
- [24] Feagin J.M. and Briggs J.S. Phys. Rev. Lett. **57** 984 (1986)
- [25] Feagin J.M. and Briggs J.S. Phys. Rev. A **37** 4599 (1988)



- [26] Rost J.M. and Briggs J.S. J. Phys. B: At. Mol. Opt. Phys. **21** L233 (1988)
- [27] Kellman M.E. Phys. Rev. Lett. **73** 2543 (1994)
- [28] Ho Y.K., Phys. Rev. A, **34** 4402 (1986)
- [29] Watanabe S. and Lin C.D. Phys. Rev. A **34** 823 (1986)
- [30] Dmitrieva I.K. and Plindov G.I. J. Physique **47** 1493 (1986)
- [31] Rost J.M., *et al.* J. Phys. B: At. Mol. Opt. Phys. **24** 2455 (1991)
- [32] Rost J.M. and Briggs J.S. J. Phys. B: At. Mol. Opt. Phys. **24** 4293 (1991)
- [33] Ho Y.K., Phys. Rev. A, **48** 3598 (1993)
- [34] Ostrovsky V.N. and Prudov N.V. J. Phys. B: At. Mol. Opt. Phys. **26** L263 (1993)
- [35] Müller J., Yang X., and Burgdörfer J., Phys. Rev. A **49** 2470 (1994)
- [36] Grémaud B. and Delande D. (to be published)
- [37] Ho Y.K., Phys. Rep. **99** 1-68 (1983)
- [38] Balslev E. and Combes J.M., Commun. Math. Phys. **22** 280 (1971)
- [39] Buchleitner A., Grémaud B. and Delande D., J. Phys. B: At. Mol. Opt. Phys. **27** 2663 (1994)
- [40] Bürgers A. and Rost J.M., J. Phys. B: At. Mol. Opt. Phys. **29** 3825 (1996)
- [41] Richter K., Tanner G. and Wintgen D. Phys. Rev. A **48** 4182 (1993)
- [42] Gaspard P., Alonso D., and Burghardt I. Adv. Chem. Phys. **XC** 105 (1995)
- [43] Grémaud B. and Delande D.(to be published)

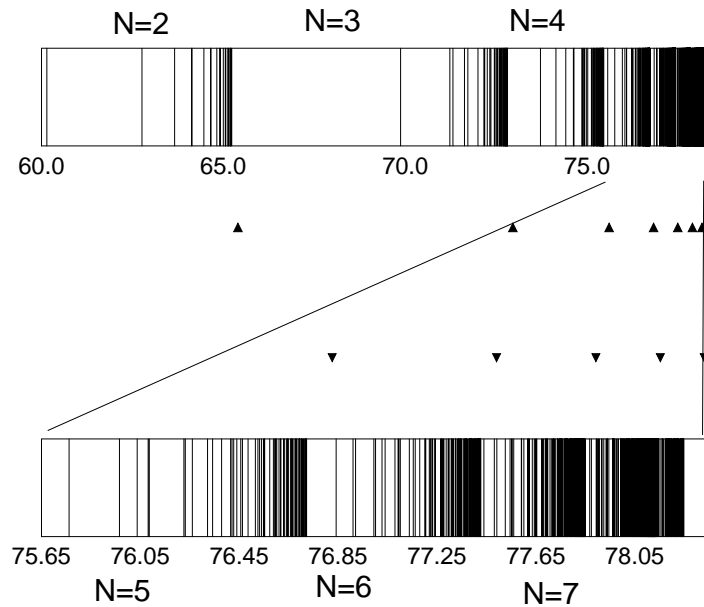


FIG. 1. Spectrum of the helium atom ( $^1P^o$  states) as it is obtained from numerical diagonalization. Energies are given in electron-Volt above the ground state. Only the resonances are shown ( $8 \geq N \geq 2$ ). It is made of Rydberg series converging to simple ionization thresholds (▲ and ▼), which are part of the Rydberg series of the  $\text{He}^+$  levels converging towards the double ionization limit ( $E = 79.003$  eV). (Because of the numerical precision, the calculated Rydberg series are truncated, so that they appear to converge to effective thresholds lower in energy). Above the  $N = 3$  threshold, the series overlap.

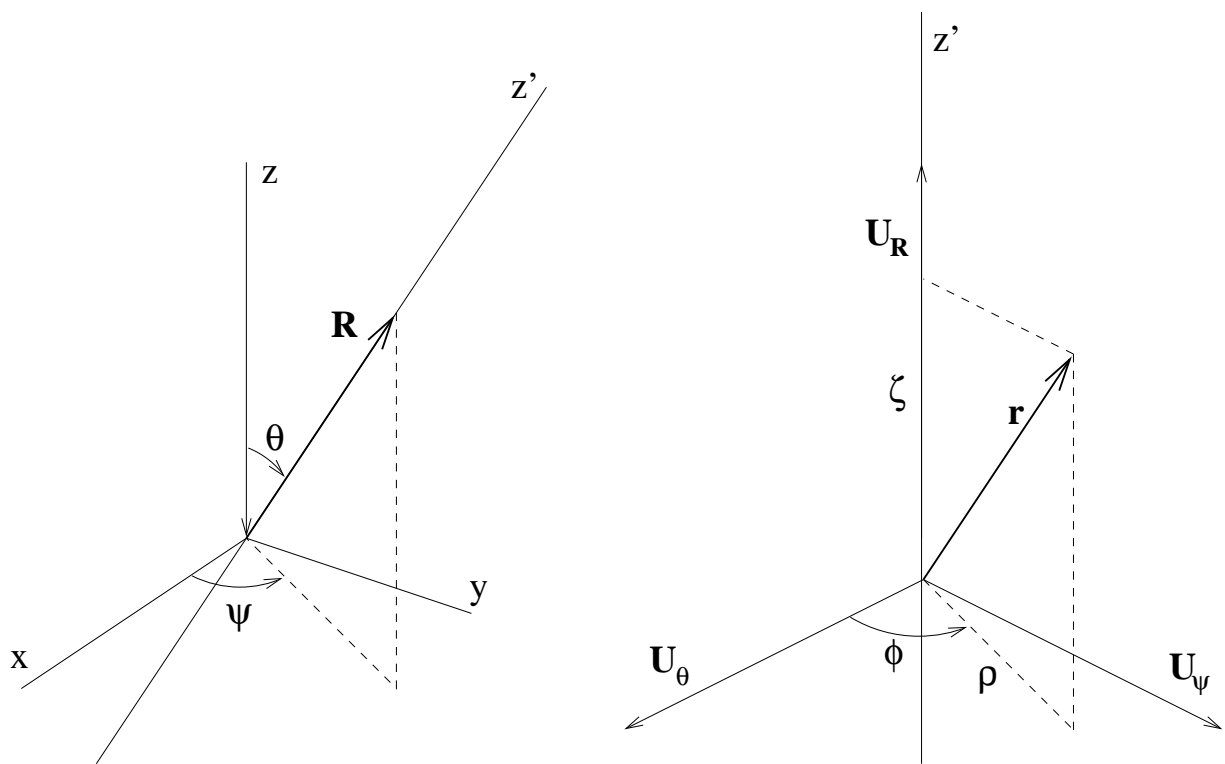


FIG. 2. Definition of the molecular-like system of coordinates.  $\mathbf{R}$  is the inter-electronic vector and  $\mathbf{r}$  is the vector from the origin to the centre of mass of the two electrons.  $\mathbf{R}$  is defined by the usual spherical coordinate  $(R, \theta, \Psi)$  and  $(\rho, \zeta, \phi)$  are the cylindrical coordinates of  $\mathbf{r}$  relative to the body-fixed axis  $z'$  defined by  $\mathbf{R}$ .

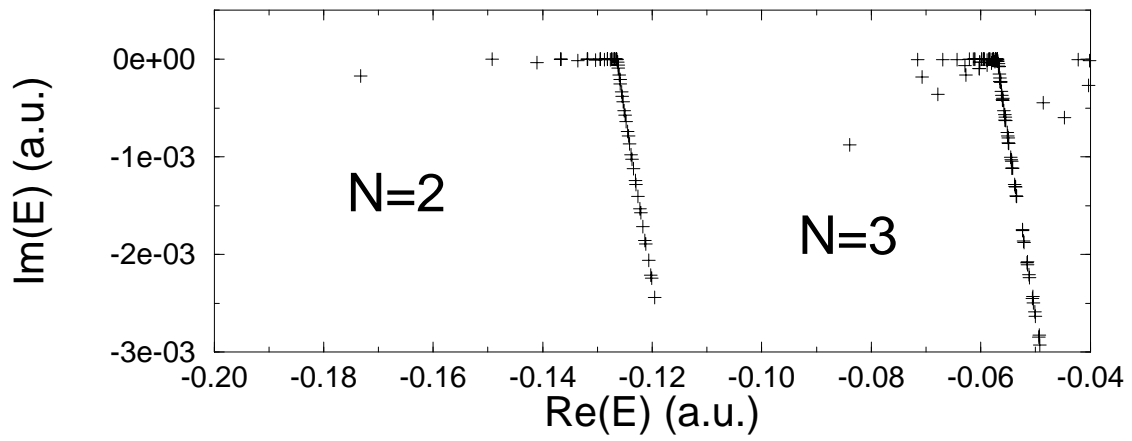


FIG. 3. Complex spectrum of  $1\mathbf{P}^o$  states of the helium atom showing the  $N = 2$  and  $N = 3$  Rydberg series. This spectrum is obtained by numerical diagonalization of the complex Hamiltonian  $H(\theta)$  for  $\theta = 0.16$ . Due to the matrix truncation, the rotated continua are discretized.

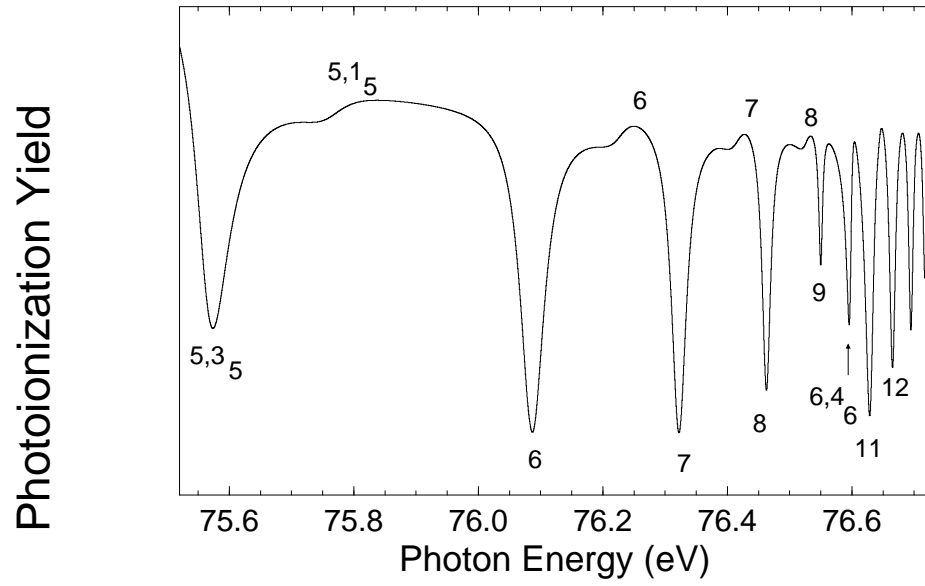


FIG. 4. Theoretical photoionization cross-section below the  $N = 5$  threshold, convoluted at the experimental resolution of reference [13]. The oscillations due to overlap with the  $6, 4_6$  member from the upper series are very well reproduced. The resonances belonging to the two main series,  $5, 3_n$  (below) and  $5, 1_n$  (top), are indicated using Lin's classification scheme. The position of the perturber coming from the  $N = 6$  series is also indicated.

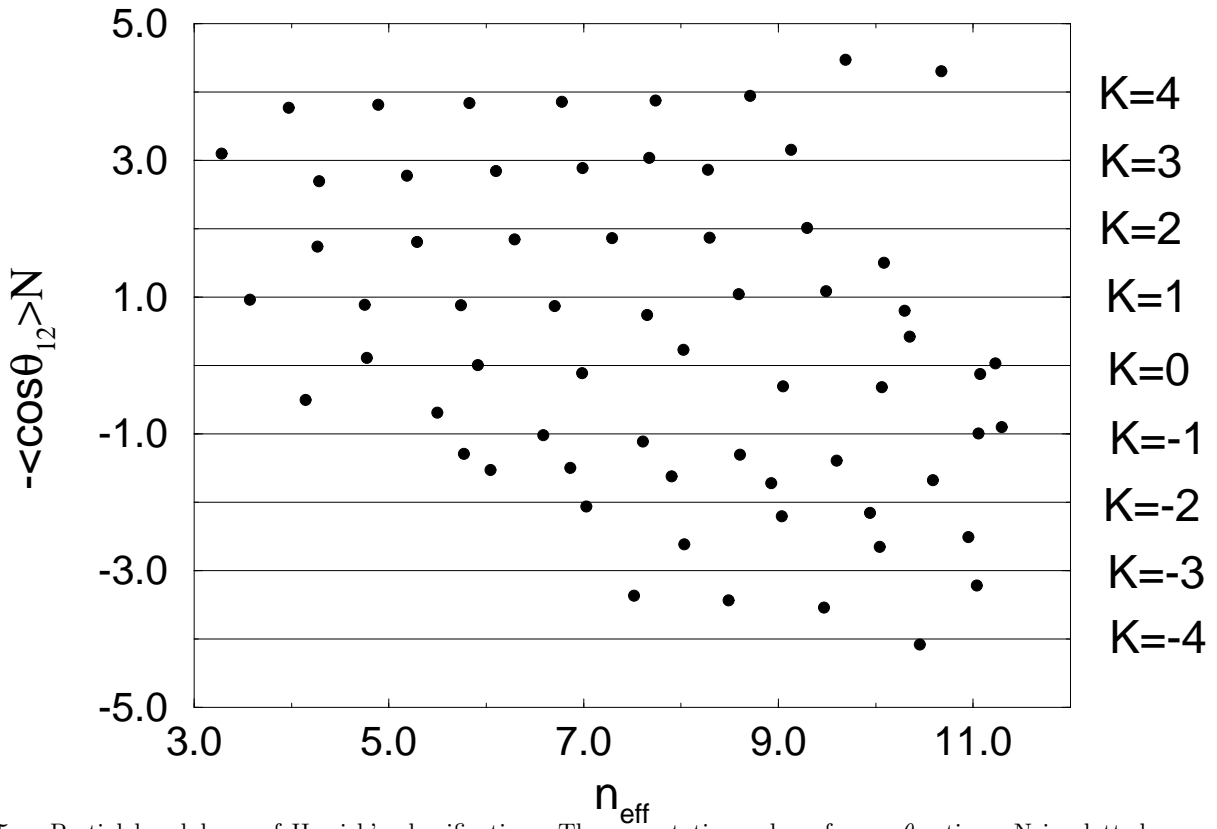


FIG. 5. Partial breakdown of Herrick's classification. The expectation value of  $-\cos \theta_{12}$  times  $N$  is plotted versus the effective quantum number  $n_{\text{eff}}$ . Although series with high  $K$  number are well separated, the others are mixing, especially in the energy range where interaction with the  $6, 4_6$  state occurs. Horizontal lines depict the values predicted by Herrick's theory.

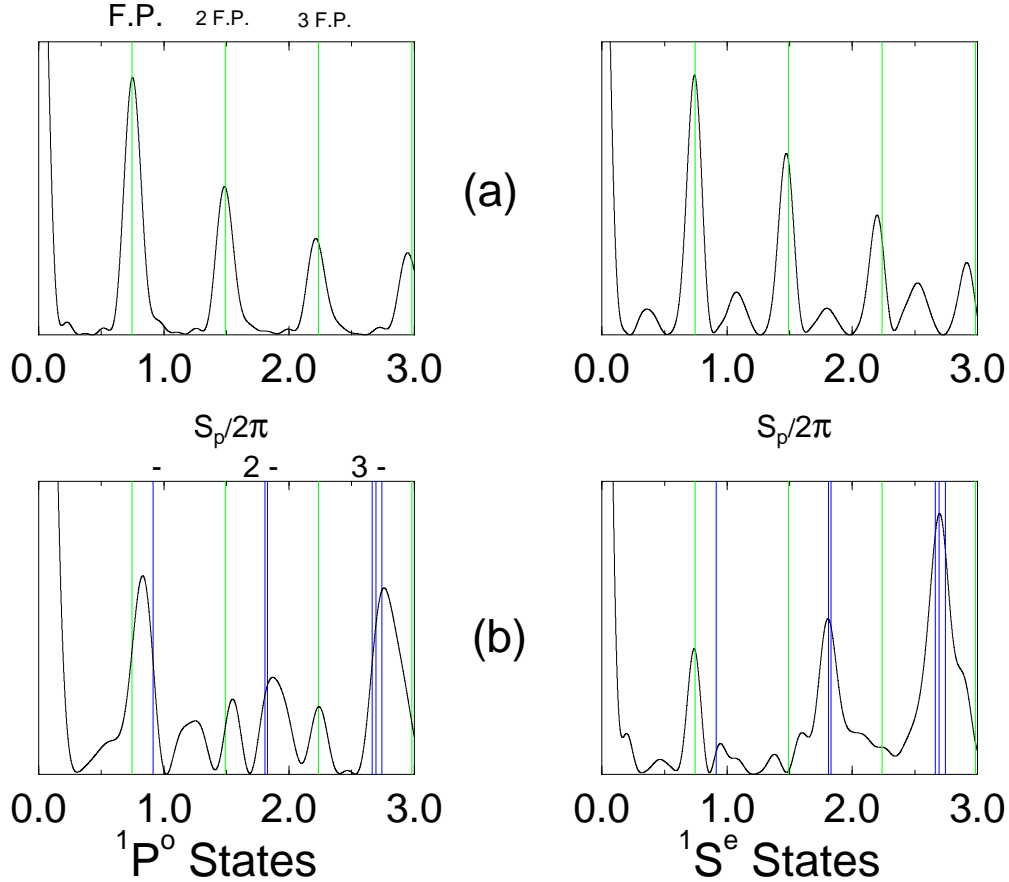


FIG. 6. Scaled spectroscopy of  $1S^e$  states (on the right) and  $1P^o$  states (on the left). The upper plots (a) depict the SFT of the Green function  $G(E)$ . The vertical lines gives the values of reduced action of the frozen-planet orbit ( $Zee$  configuration) and its repetitions. Both SFTs have peaks at those actions. The lower plots (b) depict the SFT of the operator  $\cos\theta_{12}G(E)$ . The weight of the  $Zee$  orbits have been lowered, while peaks appear at the reduced actions of three first  $eZe$  configuration orbits and their repetitions (given by the solid vertical lines, the dotted vertical lines give the repetitions of the action of the  $Zee$  orbit).  $-$  corresponds to the asymmetric stretch,  $2-$  (resp.  $3-$ ) to its second (resp. third) repetition, which is very close to the  $+-$  (resp.  $++-$  and  $+--$ ) orbit.

FIG. 7. Conditional probability density for the inner electron with respect to the fixed axis between the nucleus and the outer electron. The outer electron is at a distance of 260 atomic units, the classical expectation value for the outer electron along the classical  $Zee$  periodic orbit. This resonance belongs to the  $N = 7$  series of  $1P^o$  states. Its energy is  $-0.0113416$  atomic units (77.77 eV above the helium ground state) and its width is  $1.38 \times 10^{-6}$  (0.15 meV). The expectation value of  $\cos\theta_{12}$  is 0.73. The inner electron is clearly localized between the nucleus (0,0) and the outer electron (260,0) and the wavefunction looks very much like a hydrogenic Stark state, emphasizing the classical interpretation of a inner electron oscillating in the electric field created by the outer one.

FIG. 8. On the bottom : probability density for the two electrons at fixed inter-electronic angle  $\theta_{12} = \pi$ . This resonance is taken from the  $N = 7$  series of  $1P^o$  states. Its energy is  $-0.011564$  in atomic units (77.75 eV above the helium ground state) and its width is  $8.60 \times 10^{-9}$  a.u. (0.936  $\mu$ eV), which is very small compare to other states in the same energy domain. The expectation value of  $\cos\theta_{12}$  is  $-0.842$ . It is strongly localized around the  $-$  asymmetric stretch orbit (shown on the top of the figure), which is probably the reason of a so long lifetime.

TABLE I. Reduced actions  $S_p(E = -1)/2\pi$  of several periodic orbits of helium. Stability is with respect to displacement conserving collinearity. F.P. stands for frozen-planet, A.S. for asymmetric stretch and  $eZe$  for the other collinear orbits of this configuration .

name	code	reduced action $S_p/2\pi$	Stability
F.P.		0.7458	stable
Langmuir		0.6761	stable
Wannier		1.7500	inf. unstable
A.S.	—	0.9145	unstable
$eZe$	+—	1.8091	unstable
$eZe$	+ + —	2.6631	unstable
$eZe$	+ — —	2.6951	unstable

TABLE II. Theoretical values of resonances energies  $E$ , linewidths  $\Gamma$ , reduced linewidths  $\Gamma^*$ , reduced probabilities of transition  $P^*$  and Fano  $q$ -parameters for the two principal series below the  $N = 5$  threshold ( $5, 3_n$  and  $5, 1_n$ ).  $\Gamma$  and  $\Gamma^*$  are in meV. The reduced probabilities values are given in percentage relatively to the  $2, 0_n$  series. There are sensible changes of the properties for the states with greater energy than 76.5915 eV, the energy of the interfering state  $6, 4_6$ .

$n$	$E - E_g$ (eV)	$\Gamma$	$\Gamma^*$	$P^*$	$q$
			5, 3 <sub>n</sub>		
5	75.5639	59.09	2090	1.767	-0.225
6	76.0840	42.49	3332	3.427	-0.022
7	76.3199	25.16	3501	3.747	-0.006
8	76.4605	12.41	2813	2.987	0.006
9	76.5479	3.02	1031	1.005	0.066
10	76.5953	3.51	1588	1.043	0.537
11	76.6278	11.89	6738	8.167	0.190
12	76.6633	7.88	5998	7.596	0.046
13	76.6926	4.97	5097	6.542	0.012
14	76.7151	3.28	4438	5.870	0.024
			5, 1 <sub>n</sub>		
5	75.7590	88.82	4041	0.176	0.437
6	76.2237	57.25	6140	0.170	0.706
7	76.4131	38.10	7196	0.222	0.702
8	76.5234	22.48	6762	0.286	0.629
9	76.5941	11.16	5000	0.707	0.023
10	76.6422	4.35	2762	0.002	0.990
11	76.6754	0.64	550	0.006	0.737
12	76.6980	0.41	447	0.002	-1.880